4
Experimental results

In order to perform the experimental tests, a test bench was made (fig. 4.2) based on the model proposed in section 2 (fig. 4.1).

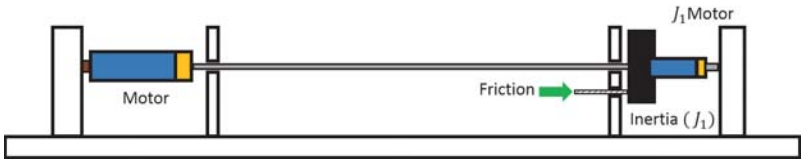

Figure 4.1: Mechanical model with an extra motor on J_1

This apparatus is proposed to study only the rotational and torsional dynamics of the system, for that reason the motor and the inertia are mounted on bearings so that the setup can be used in an horizontal position, making it easy to operate and troubleshoot eventual problems. The drill string is 2.4m long and is made of a 3mm diameter steel rod.

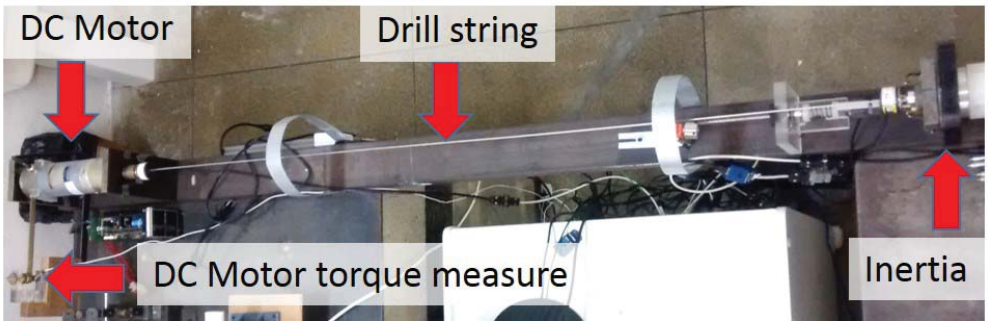

Figure 4.2: Experimental setup

The DC motor (fig.4.3) is mounted on two ball bearings, so the torque applied by the motor is obtained through a force measured by a load cell positioned at a known distance from the motor.

The drill string is locked on the Inertias by a 3-jaw chuck (fig.4.4), this way we can use different diameter rods and substitute them easily with a chuck drive maintaining the centering of the system.

Initially, only two optical incremental encoders were used to measure the angle of the motor and the inertia and then this angular measurement was differentiated to obtain the angular speeds. That approach led to a problem of

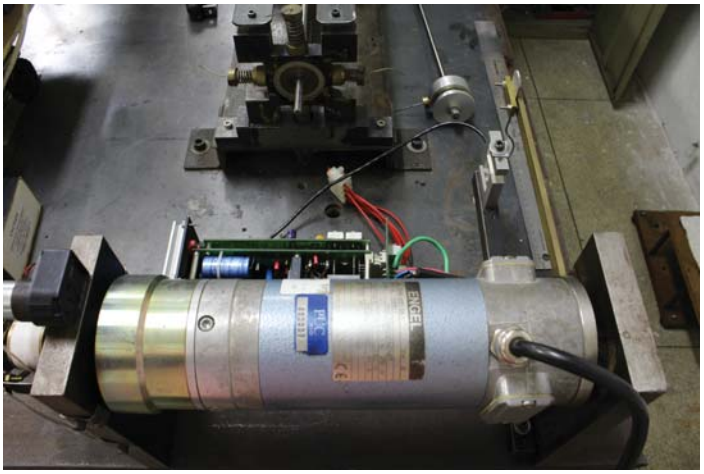

Figure 4.3: Top drive DC motor

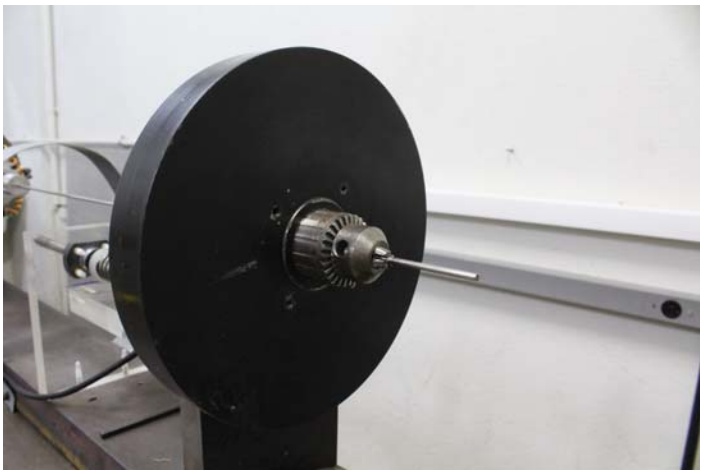

Figure 4.4: Inertia chuck

very high measurement noise due to the differentiation process. Therefore, a tachometer was added to the DC motor and on the inertia to measure the actual angular speed and the encoders were used to measure the angles only (fig. 4.5). This approach led to a 3 times lower measurement noise when compared to the differentiation process.

The torque applied by the main motor, the normal force of the brake on the inertia, and the rotational speed of the motor and of the inertia, are measured and the data recorded by a National Instruments cDAQ system.

A second, smaller DC motor with 128:1 planetary gearbox can be attached to the inertia J_1 (fig. 4.6) to add, in addition to the dry friction induced by the pin, a controllable torque to J_1. This motor is controlled directly from the PC running LabView by a transparent serial wireless link and it is powered by a Lithium Polymer (Li-Po) Battery in a way that all this system is attached to J_1 and it can rotate freely. This approach of using a battery and

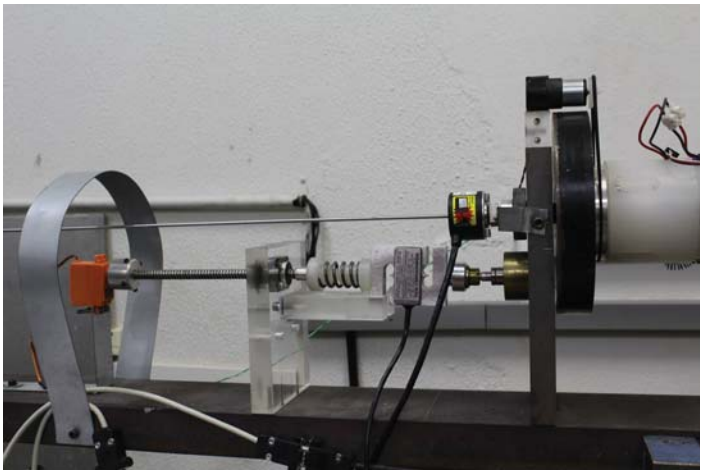

Figure 4.5: Incremental encoder (left of inertia) and tachometer (belt driven on right of inertia)

a wireless data link was preferred to avoid the use of slip rings, that are more susceptible to noise and cannot transmit high currents.

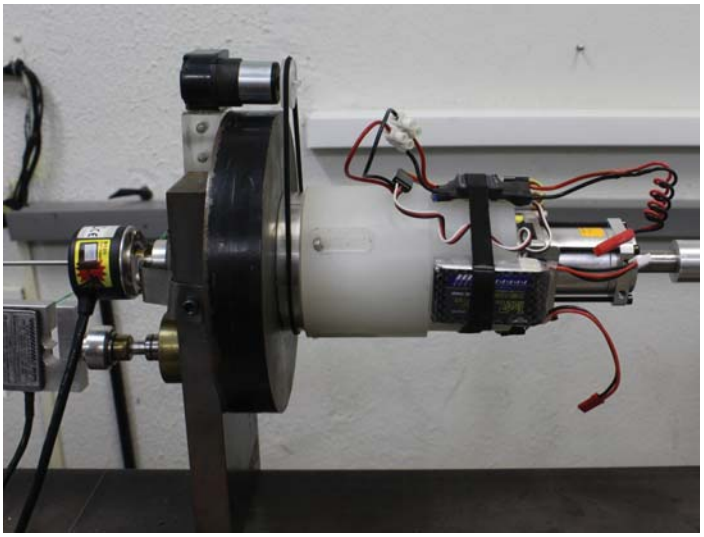

Figure 4.6: DC motor on J_1

Figure 4.7 shows a diagram of the electronic components used to drive and control the motor in the J_1 inertia. This motor speed is controlled by the same LabView program that acquires data from all the sensors in the test bed and actuates the main DC motor. As the motor is positioned on the J_1 inertia that is a rotating body, it utilizes a wireless data transmission system to transmit the desired speed from the control PC running LabView to the motor.

The system uses a pair of 433 MHz SiK data link radio, the "ground" unit is connected to the PC trough a FTDI serial-to-USB converter. The other unit

is connected directly to the micro controller serial port. This micro controller receives the desired speed as a string trough serial connection and converts it to a low voltage pulse width modulation (PWM) signal that is sent to the speed controller.

The speed controller is essentially a MOSFET H-Bridge that receives the low voltage PWM from the micro controller and modulates, using a high power PWM, the output voltage applied to the motor. All this system is powered by a 3 cell Lithium Polymer battery, that provides around 12V to the system. The power consumed by the motor during the tests is not sufficient to cause a significant voltage decay on the battery, so the supply voltage is considered constant for the duration of the tests, which is usually a few minutes.

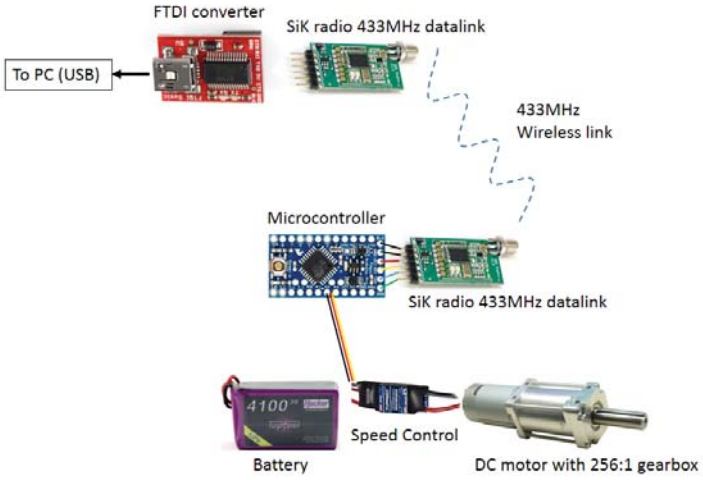

Figure 4.7: Electronic diagram of the J_1 motor

4.1 Mechanical properties of the experimetal setup

The most important mechanical parameters to be determined are the torsional stiffness of the drillstring (K), and the inertia (J_1), but the mathematical models also need the bearing losses b_1 and b_m and the damping from internal losses in the drillstring. The stiffness of the drillstring can be analytically calculated trough the equation:

$$K = \frac{GI}{L} = 0.268 Nm/rad \tag{4.1}$$

where G is the shear modulus, I is the moment of inertia of the cross section, and L is the length of the drillstring. The shear modulus G and the moment of inertia I are:

$$G = \frac{E}{2(1+v)} \qquad I = \frac{\pi}{32}D^4 \tag{4.2}$$

Where D is the diameter of the shaft and v the Poisson ratio. Table (4.1) shows the mechanical properties of the drillstring.

Parameter	**Value**	**Unit**
String length (L)	1.7	m
String density (ρ)	7850	kg/m^3
String diameter (mm)	3	mm
Young modulus (E)	210	GPa
Poisson ratio (v)	0.3	-

Table 4.1: Mechanical parameters of drillstring

The inertia rotor J_1 is composed by a thick steel disc, the small DC motor attached to J_1, its driver electronics and battery. The inertia of all these components are summed and referred as J_1 in this thesis, unless specified. The mechanical properties of this set are described in table (4.2).

Parameter	**Value**	**Unit**
Mass of steel disk	4.556	kg
Mass of DC motor with gearbox	1.148	kg

Table 4.2: Mechanical parameters of J_1

The moment of inertia of the components of J_1 were analytically calculated by:

$$J_1 = \frac{1}{2}Mr^2 \tag{4.3}$$

And the obtained results are:

Parameter	**Value**	**Unit**
Inertia of steel disk	0.01494	kgm^2
Inertia of DC motor with gearbox	0.00064	kgm^2
Total inertia of J_1	0.01555	kgm^2

Table 4.3: Inertias of J_1

In order to obtain experimentally the stiffness of the drillstring to ensure the material proprieties of the string, a static test was performed. Figure 4.8 shows the dynamometer used to measure the applied force (and knowing the

distance) the torque on the rotor. The displacement is acquired by the rotary encoder and read through the data acquisition system.

Figure 4.8: Experimental torque measurement

Results for this test are shown in table (4.4)

Torque (Nm)	**Angle** (rad)	**K** (Nm/rad)
0.1136	0.4448	0.2553
0.2216	0.8832	0.2509
0.2521	0.9736	0.2583

Table 4.4: Experimental stiffness of drillstring

An average stiffness $K = 0.2548 Nm/rad$ was obtained which, compared with the result of the stiffness analytically calculated from equation (4.1), has a difference of 5.18%. Although small this difference can impact the results, so the experimentally calculated stiffness was the one used in the models for simulations, in order to obtain numerical results that are closer to the experimental setup.

The parameters of the top drive DC motor were obtained from the manufacturer datasheet. The motor is an Engel GNM 5480 42V with planetary 8:1 gearbox.

Parameter	**Value**	**Unit**
Moment of inertia of motor (J_m)	0.37×10^{-3}	kgm^2
Armature inductance (L_{DC})	1.10×10^{-3}	H
Armature resistance (R_{DC})	0.33	Ω
Torque constant (K_t)	0.12	Nm/A
Speed constant (K_e)	6.02×10^{-2}	$V/(rad/s)$
Dry friction torque (T_f)	0.1	Nm

Table 4.5: DC motor parameters

In order to obtain the natural frequency of the system and the damping coefficients the following test was performed. The DC motor was mechanically locked and then an angular displacement was imposed on the inertia J_1. J_1

was then released and its speed was acquired with the data acquisition system. Figure 4.9 shows the simple oscillator decay over time.

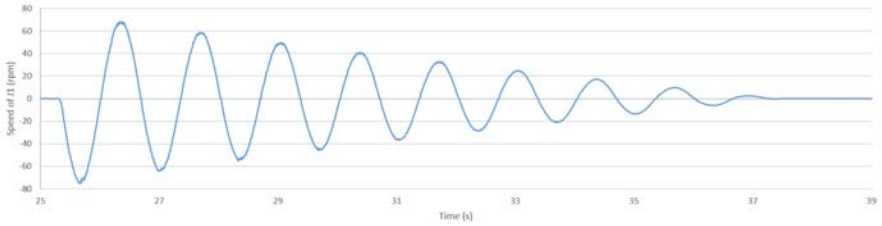

Figure 4.9: Time response of the system with initial displacement

Using this graph information, the damped frequency of the system (ω_d) was calculated to be $0.751Hz$. To calculate the natural frequency of the system (ω_n) we use equations 4.4,4.5,4.6.

$$\delta = \ln \frac{x_1}{x_2} \tag{4.4}$$

$$\xi = \frac{\delta}{\sqrt{(2\pi)^2 + \delta^2}} \tag{4.5}$$

$$\omega_n = \frac{\omega_d}{\sqrt{1 - \xi^2}} \tag{4.6}$$

where x_1 and x_2 are two successive amplitudes of the peaks on fig. (4.9). Trough this equations we calculate the natural frequency of the system ω_n,

δ	ξ	$\omega_d(Hz)$	$\omega_n(Hz)$
0.1488	0.0236	0.7518	0.7520

Table 4.6: Frequencies and damping of the system

As the drillstring stiffness is a very important parameter on the characterization of the experimental setup, another test was performed to measure the torsional stiffness of the string. The top drive motor was kept static and the inertia J_1 was turned to one side, back to the center, and then to the other direction as fig. (4.10)

Figure 4.11 shows a plot of the measurement of the load cell that measures the torque on the top drive motor vs the angle between J_1 and the top drive, as a response to the angle input shown on fig. (4.10). As one can note, the graph is very much linear, showing that the stiffness of the drillstring is linear as expected. It is also notable that there is no significant hysteresis on the measurement of the load cell, what indicates that the mechanical setup that

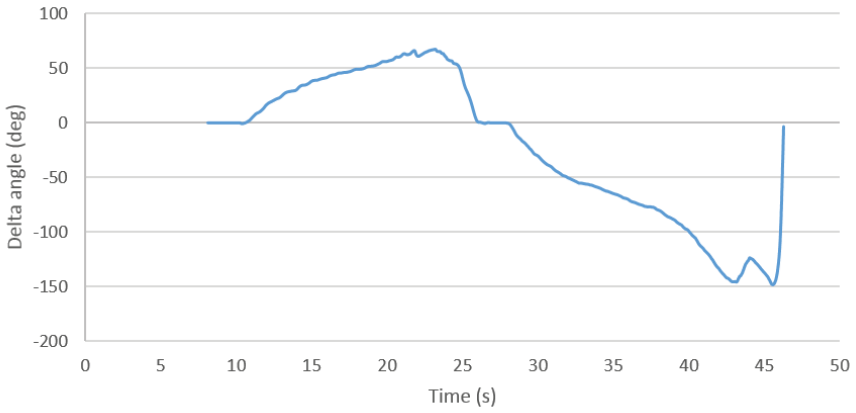

Figure 4.10: Angle displacement between J_1 and top drive over time

supports the top drive motor has no important friction on the bearings that could add some hysteresis to the measurements. The red dot line is a linear regression of the measurements and its equation $y = 6e^{-5}x + 0.0046$

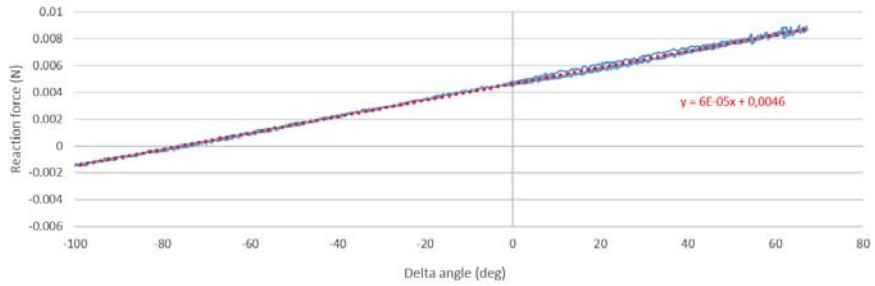

Figure 4.11: Force as a function of the angle between J_1 and top drive

After multiplying the force measured on the load cell by the perpendicular distance that it is positioned to the motor we can have the torque. Converting the result force vs. angle equation $y = 6e^{-5}x+0.0046$ to torque we measured the torsional stiffness being 0.266 Nm/rad. The difference between results obtained by graph 4.11 and table 4.4 are mainly from the friction present on the bearing of the motor mount that holds part of the reaction torque, not passing all to the load cell that measures it.

4.2 Sensors analysis

Two different sensors were used to measure the angular velocity in the test, this section intends to compare in a qualitative way both of them in order to indicate which one is more adequate to be used for registering the angular

velocity of the experimental tests. As these two sensors were already available in the lab, buying different ones was not considered for this work.

The first one is an AVAGO tachometer, this sensor outputs an analog DC voltage level that is linearly proportional to the angular velocity of the input shaft. On the buildup, they are connected to the motor and J_1 trough flexible belts, and as they have little inertia and internal friction, we can assume there is no sliding and therefore the RPM relation between the sensor and the system is fixed by the relation of diameters of the pulleys. Figure 4.12 shows them inside the red boxes.

The second sensor used is an LS Mecapion H40-8-1000VL, that is an optical quadrature encoder. This type of sensor outputs two square waves (A and B) in witch digital pulses (fig. 4.13 represent that the shaft turned $1/PPR$ revolutions, where PPR are pulses per revolution. The number of PPR determinate the angular precision of the sensor, the sensor used on this buildup has 1000 PPR and can be seen in fig. 4.12 in the yellow boxes.

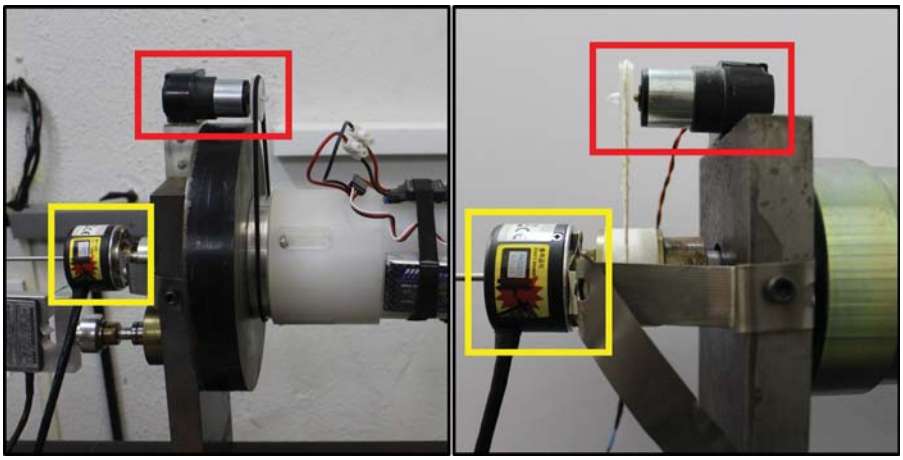

Figure 4.12: Encoders and tachometers in J_1 (left) and Top drive motor (right)

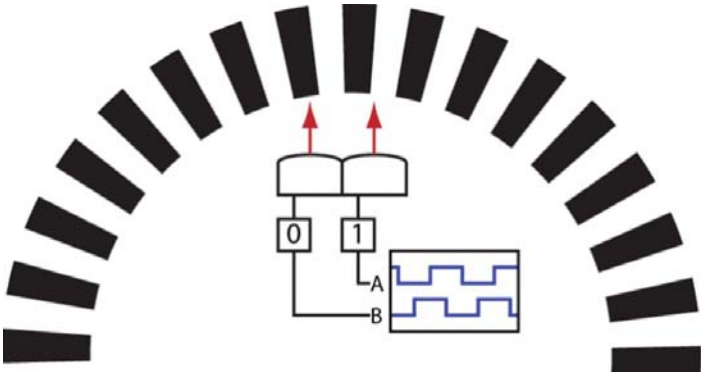

Figure 4.13: Quadrature encoder

As one can note, to obtain the angular speed from the optical encoder, the data acquisition system must count the pulses received, divide by the number of pulses per revolution to obtain an measured angle, and then differentiate over time to obtain the angular speed (eq. 4.7).

$$\omega = \frac{d\theta}{dt} \tag{4.7}$$

The problem associated with this approach of differentiate the angle over time is that this process adds a lot of noise on the measurement. Therefore, a series of experimental tests were performed on the test buildup to compare the results obtained from both sensors. Figure 4.14 shows the tachometer measurement of angular velocity on a test where the motor was set to a constant RPM and 25s were elapsed from the beginning of the test so that the system stabilizes on its steady state.

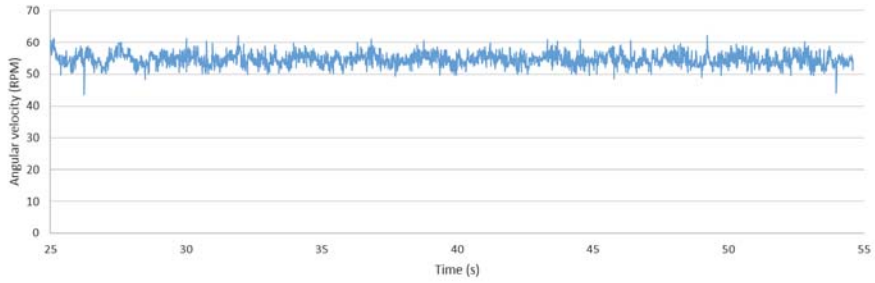

Figure 4.14: Tachometer measurement of angular velocity (RPM)

Figure 4.15 shows the measurements of the angular velocity made by the optical encoder using the differentiation over time method, this data was acquired from the same test shown in fig. 4.14.

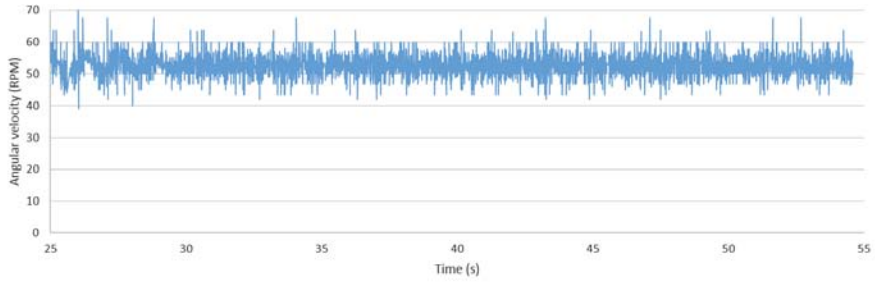

Figure 4.15: Optical encoder measurement of angular velocity (RPM)

One can see that the measurement of the tachometer has much less noise than the one made by the optical encoder. Figure 4.16 shows the difference in % between the encoder and tachometer measurements.

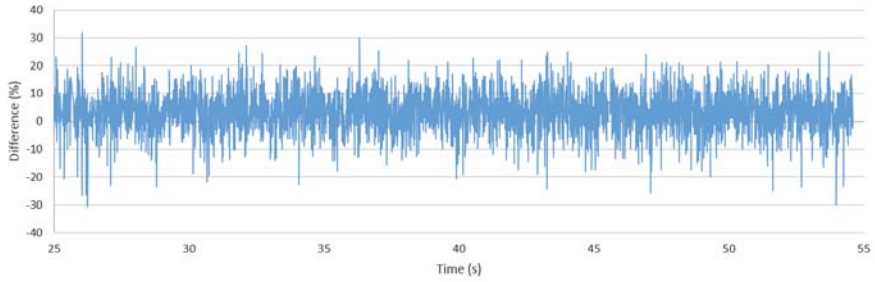

Figure 4.16: Percentual difference between encoder and tachometer measurements.

From this results, the mean, standard deviation and variance of both signals were calculated assuming a constant speed of the motor during the tests, results can be seen in Tab. 4.7.

Item	Value	Unit
Variance of Tachometer	4.591	RPM
Variance of Encoder	15.833	RPM
Mean of Tachometer	54.574	RPM
Mean of Encoder	52.637	RPM
Standard deviation of Tachometer	2.142	RPM
Standard deviation of Encoder	3.979	RPM

Table 4.7: Statistical analysis of angular velocity sensors

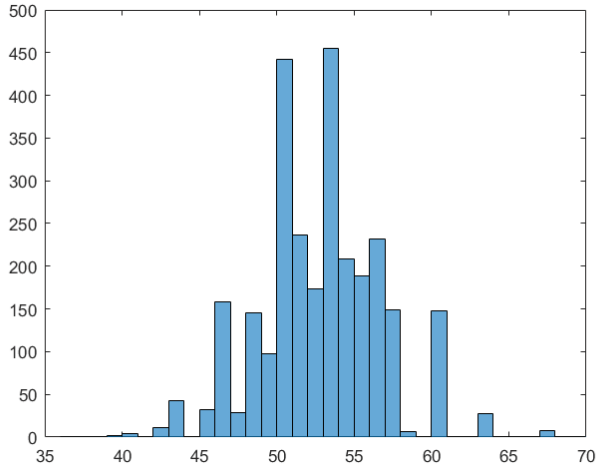

Figure 4.17: Histogram of motor encoder measurements

From tab. 4.7, one can see that the variance of the measurements on the tachometer are one third of the variance on the encoder measurements. Also, the deviation of the encoder, is almost double the one from the tachometer.

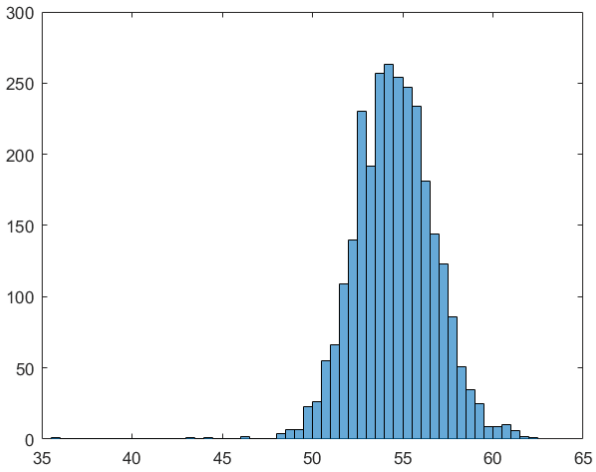

Figure 4.18: Histogram of motor tachometer measurements

The difference on the mean on the other hand, has a much lower difference that could be even reduced using more precise calibration of the sensors.

These tests were also performed for a different speed, in order to obtain the variation of the statistical parameters for other range of operation of the sensors. This second test was performed the same way as the first, the system without the dry friction on J_1 was accelerated to aprox. 100 RPM and after it entered its steady state, measurements were recorded with the data acquisition system.

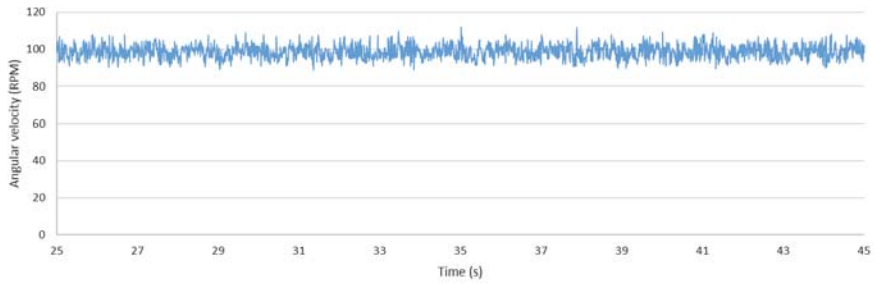

Figure 4.19: Tachometer measurement of angular velocity (RPM)

Figure 4.19, shows the measurements over time for the angular velocity using the tachometer.

Figure 4.20 shows the measurements of the angular velocity made by the optical encoder using the differentiation over time method,

As it happened on the tests performed at aprox. 55RPM, the tachometer measurements have much less noise than the one made by the optical encoder.

From tab. 4.8, one can see that the variance and standard deviation of both measurements increased when compared to tab. 4.7.

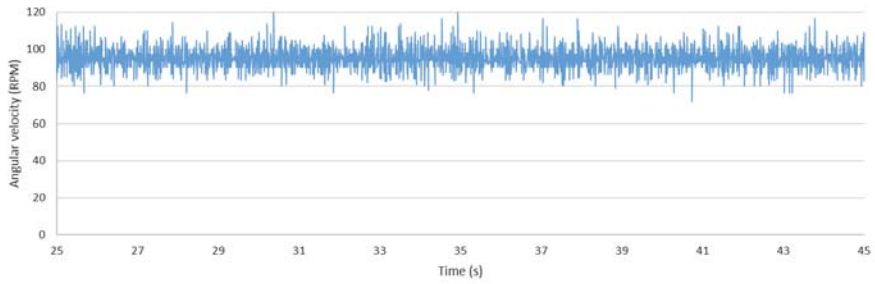

Figure 4.20: Optical encoder measurement of angular velocity (RPM)

Item	Value	Unit
Variance of Tachometer	14.922	RPM
Variance of Encoder	43.801	RPM
Mean of Tachometer	98.634	RPM
Mean of Encoder	95.219	RPM
Standard deviation of Tachometer	3.862	RPM
Standard deviation of Encoder	6.618	RPM

Table 4.8: Statistical analysis of angular velocity sensors

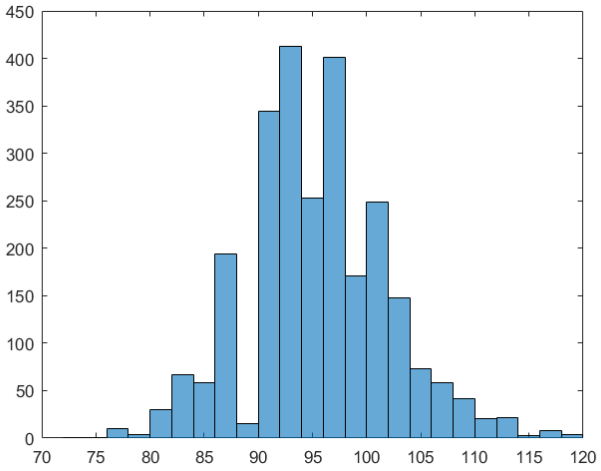

Figure 4.21: Histogram of motor encoder measurements

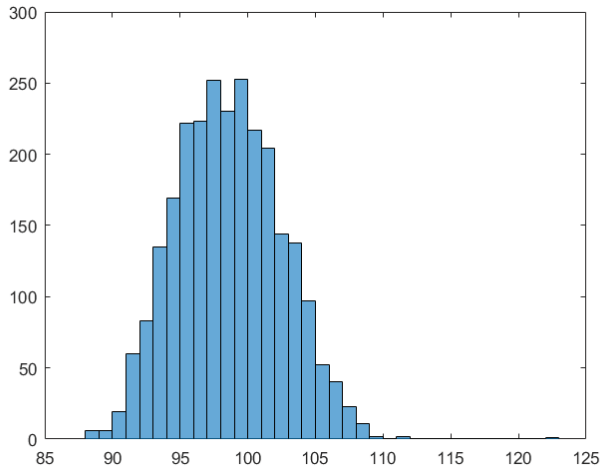

Figure 4.22: Histogram of motor tachometer measurements

Histograms of encoder and tachometer measurements for this bigger speed show a similar behavior as before, measurements made with the tachometer have a more grouped dispersion, closer to a normal distribution, and measurements made with the encoder have two dominant peaks, and a less uniform distribution.

4.3 Dynamical behavior based control

By analyzing the structure of the friction law eq.(2.14) and the results of the simulations, an investigation was started to analyze if adding a torque source to J_1 (a kind of downhole motor), it could be possible to modify the stick slip phenomenon. Using this supposition an analysis was made to verify if it is possible to mitigate the stick slip by controlling the torque on J_1 with the use of a DC motor.

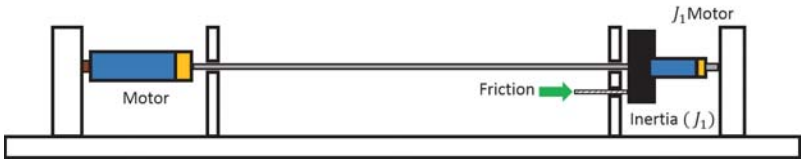

Figure 4.23: Mechanical model with motor on J_1

A recent study from Shor [43], showed that the propagation effects on torsional vibrations are important for the implementation of torsional vibrations mitigation techniques, which led to suppose that the phase of the proposed control for an imposed torque on J_1 should be important for the results. Therefore, it was simulated the lumped masses system described in

section 2 with two torque sources, both DC motors referred as "Motor" and "J_1 Motor" in fig. (4.23). The simulations started at $t = 0s$ with angular displacement and speed of the drill string being zero. At $t = 0$ the top drive motor is started at 2 rad/s, at around $t = 9s$ the energy accumulated on the drill string is enough to overcome the static friction force and the stick slip phenomenon begins. At $t = 15s$ a second DC motor attached to J_1 is energized applying a torque of aprox. $-0.29Nm$ to J_1. This method only observes the output (angular speed at J_1) to start the motor in J_1, then this control is an open loop scheme, only applying a constant torque on J_1. The torque applied on J_1 therefore is: 0 Nm for $t < 15s$ and $t > 30s$, and $-0.29Nm$ between $t = 15s$ and $t = 30s$. Results are shown in Fig.(4.24, 4.25)

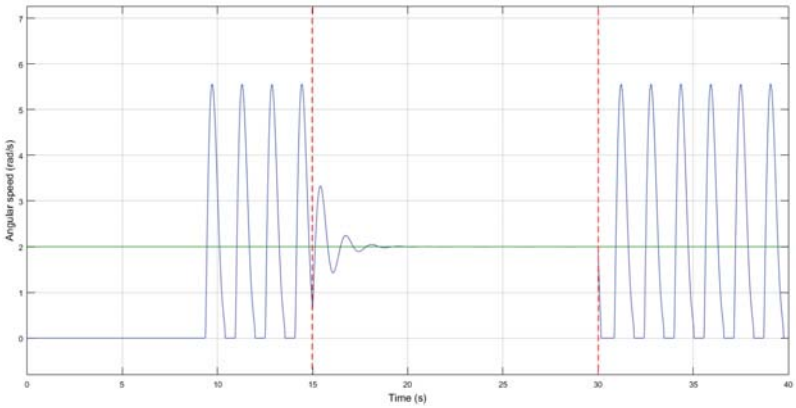

Figure 4.24: Angular speed on top drive (green) and J_1(blue)

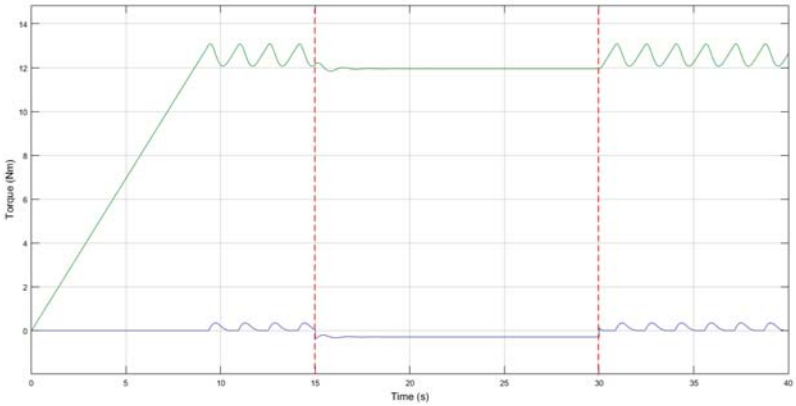

Figure 4.25: Torque on top drive (green) and J_1(blue)

As described by Shor [43], the delay effects from the propagation of torsional vibrations along the drill string must be considered for the control structure of the problem. To prove that the developed mathematical model is capable of representing these effects, the system described in Fig.(4.24, 4.25), was also simulated for a torque on J_1 being applied from $t = 14s$ to $t = 30s$.

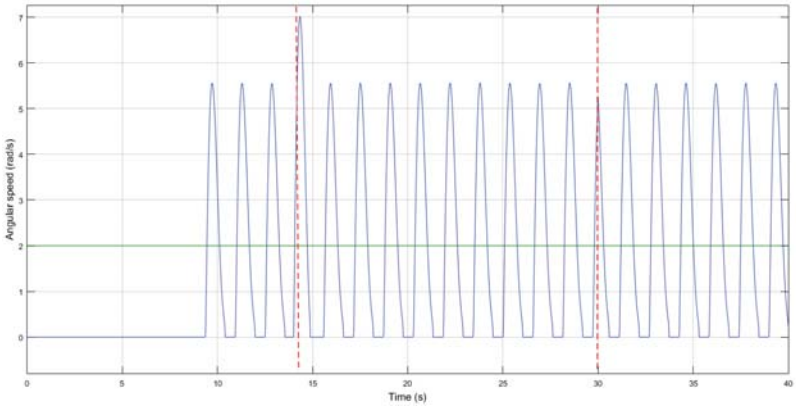

Figure 4.26: Angular speed on top drive (green) and J_1(blue)

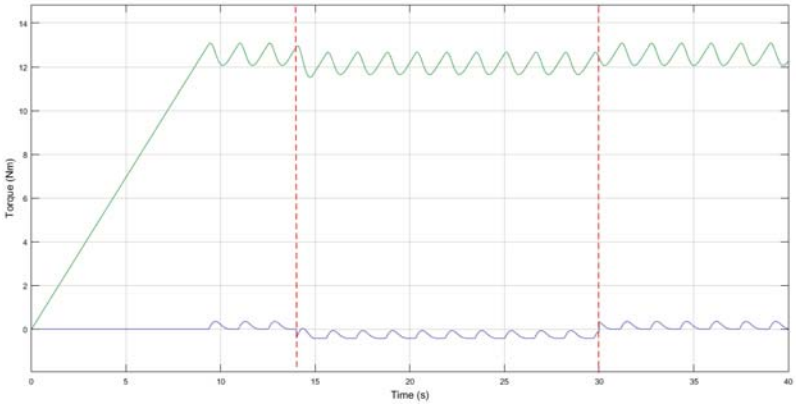

Figure 4.27: Torque on top drive (green) and J_1(blue)

Results in Fig.(4.26, 4.27) show that if the torque on J_1 is applied at a wrong moment it will have no effect on the stick-slip, only adding a small disturbance on the angular speed when it is applied. Simulations show that this approach to mitigate the stick slip only works if the torque on J_1 is applied when the angular speed of J_1 is decreasing, i.e. $\ddot{\theta}_1 < 0$.

In order to test this supposition, the same system was simulated again with the beginning of application of torque in J_1 at $T = 13.25s$.

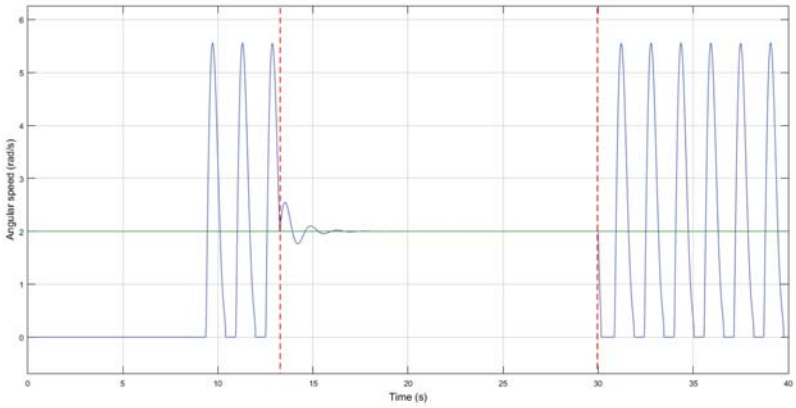

Figure 4.28: Angular speed on top drive (green) and J_1(blue)

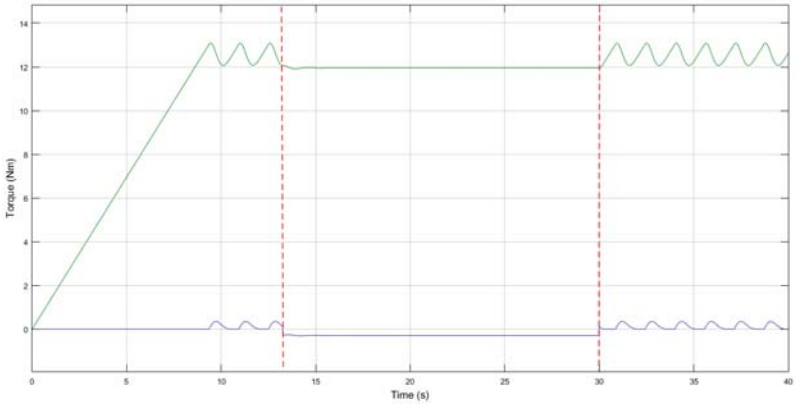

Figure 4.29: Torque on top drive (green) and J_1(blue)

Simulation results in Fig.(4.28, 4.29) show that the closer to the top drive speed is to the speed on J_1 when the torque on J_1 is applied, the better results are obtained. This is valid considering that the torque on J_1 is applied when the angular speed of J_1 is decreasing, i.e. $\ddot{\theta_1} < 0$.

It is valid to note that despite this strategy is valid, and shows good results, it depends on a precise measure of the speed on the bit (J_1) which limits its application for real life oil drilling problems with the existing technologies of bottom hole measurement available.

If, on the other hand, a positive torque is applied when the system is accelerating i.e. when the angular speed of J_1 is increasing, i.e. $\ddot{\theta_1} > 0$, the results stay the same, the stick-slip is eliminated, but in this case another phenomenon is observed. When the motor in J_1 is turned off, the system has a torsional perturbation, but it does not come back to a stick-slip behavior. Figure 4.30 shows the angular speed of the top drive and J_1, and fig. 4.31 shows the torque of both motors. As in the previous case, it is worth to note

that the torque applied by the motor in J_1 is much smaller than the one from the top drive.

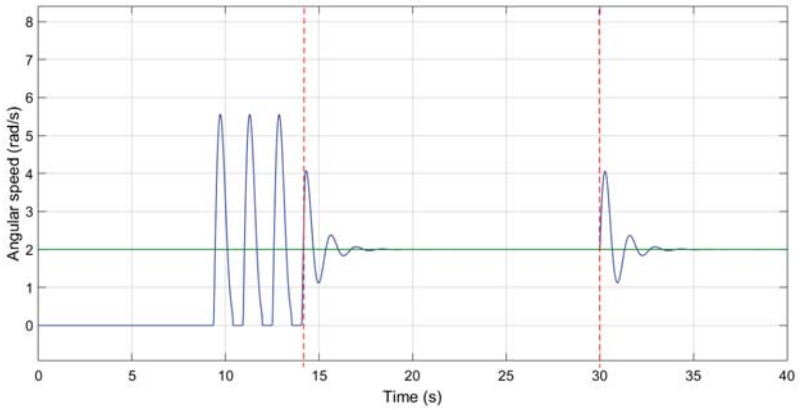

Figure 4.30: Angular speed on top drive (green) and J_1(blue)

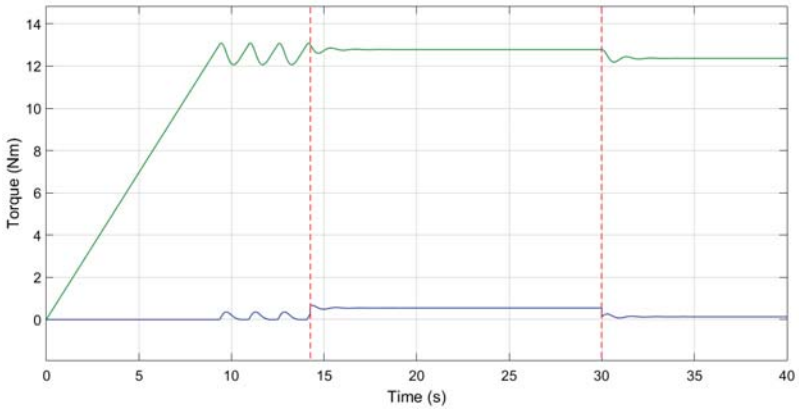

Figure 4.31: Torque on top drive (green) and J_1(blue)

Figure 4.32 shows the results obtained with the experimental setup shown in Fig. (4.2). In blue, on the left axis is the angular speed in RPM of J_1, in orange on the right axis is the amplitude of the torque in Nm applied by the DC motor attached to J_1. Results shown are very similar to the ones obtained with the numerical model. The torsional vibration on the experimental test rig is not completely eliminated due to noise on the sensors and to non-modeled imperfections of the apparatus. But this approach shows that it can eliminate the stick-slip during the period the DC motor is being used.

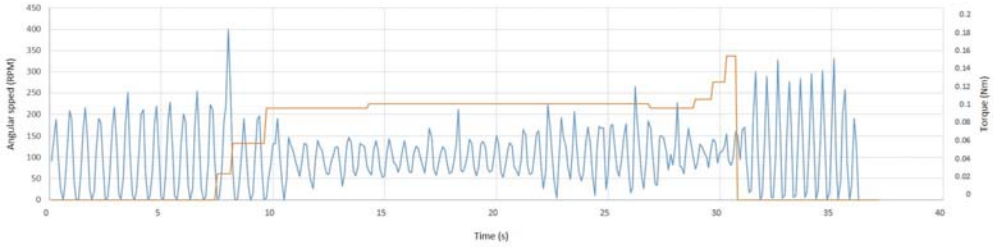

Figure 4.32: Experimental results for torque applied on J_1 in green and speed at J_1 in orange

This way, it becomes clear that the results obtained with the simulations presented in this section also happen in the experimental setup, what shows that the mathematical models are representative of the experimental setup dynamical behavior.

4.4 Influence of top drive speed on stick-slip

The influence of the top drive speed on the behavior of the stick-slip was analyzed experimentally in the experimental torsional slender setup presented. For the test presented in this section, only the top drive is active (J_1 motor is not used) and no control is applied.

This test is performed applying increasing steps of angular velocity to the top drive up to a maximum of 60 RPM and back to 0 RPM at the end. Figure 4.33 shows the results for experimental tests where the angular speed of J_1 is drawn in blue, the set point speed of the top drive in red and the measured speed of the top drive in orange. In this case there is no active control acting on the system, and the friction normal force is maintained constant during all the tests. It is possible to observe that the maximum speed of the bit (J_1) is constant up to 100s, i.e. varying the speed of the top drive from 20 RPM to 40 RPM, although the behavior of the stick slip varies, the maximum speed on the bit is very similar. On the other hand, by increasing the top drive speed from 40 to 45 RPM the maximum speed on the bit almost doubles, going from around 70 to 120 RPM. Observing the transition in 155s from 55 RPM to 60 RPM, an interesting phenomenon happens, the stick slip disappears and the amplitude of the torsional vibrations reduces.

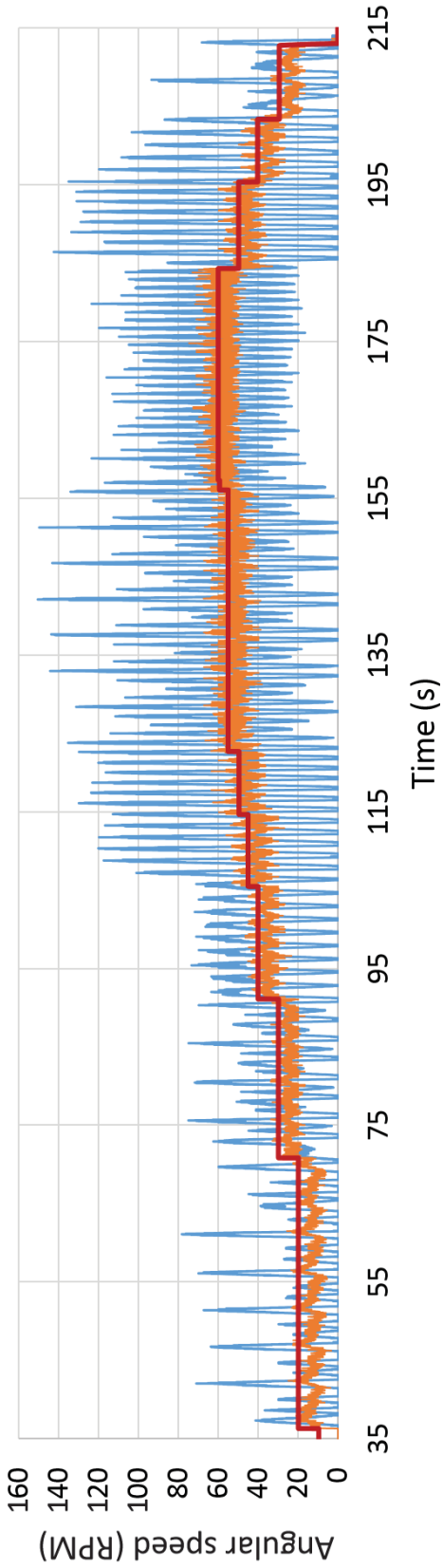

Figure 4.33: Influence of top drive speed on stick-slip

Figure 4.34 shows a zoom of the same test from 35s to 100s. During this period, the angular velocity of the top drive increases from 20 RPM, to 30 RPM and 40 RPM in the end. One can see that the peaks of maximum angular velocity have the approximate same value (around 70 RPM) for the top drive speeds varying from 20 RPM to 40 RPM. There is a periodic behavior of a bigger peak followed by two smaller ones. As the speed of the top drive increases the two smaller peaks increase, but no significant change is seen on the bigger ones. At 40 RPM the smaller and bigger peaks have both the same amplitude. One can also see that the frequency of the stick-slip oscillations doesn't change during the tests.

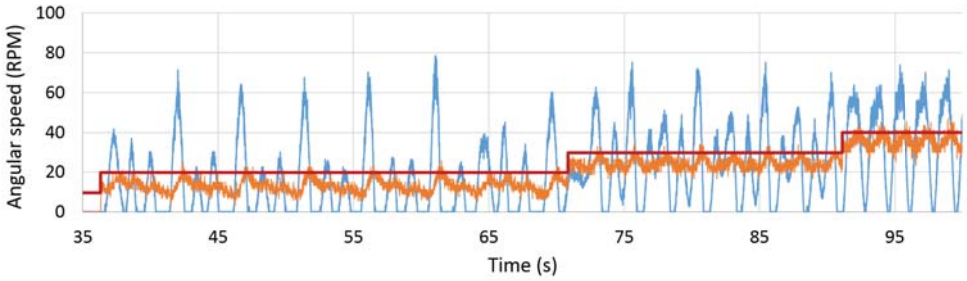

Figure 4.34: Influence of top drive speed on stick-slip from 35s to 100s

Figure 4.35 shows a zoom of the test from 100s to 114s, where the angular speed of the top drive increases from 40 RPM to 45 RPM. This increase of 5 RPM in the top drive speed makes the peaks of the angular velocity of J_1 increase from approximately 60 RPM to 110 RPM, therefore a small increase on the speed of the top drive made the maximum speed of J_1 almost double its value.

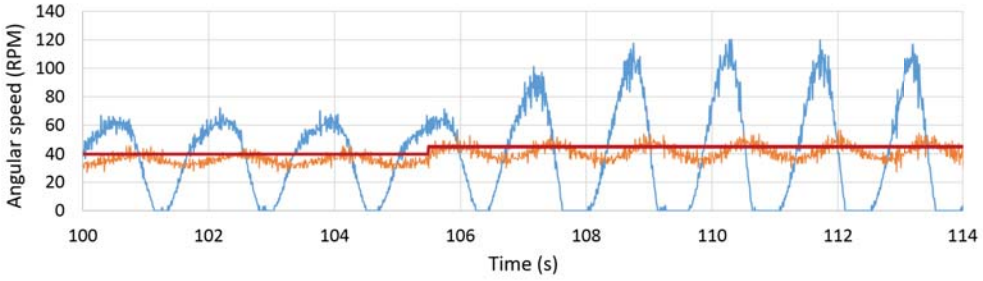

Figure 4.35: Influence of top drive speed on stick-slip from 100s to 114s

From 115s to 150s (fig. 4.36) the top drive speed is increased from 50 RPM to 55 RPM. At 55 RPM the angular velocity of J_1 still has a very short

"stick" phase, where the angular velocity is zero, but the behavior of having two oscillations of smaller amplitude reappears, but differently from fig. 4.34, the two smaller amplitude oscillations does not have a "stick" phase.

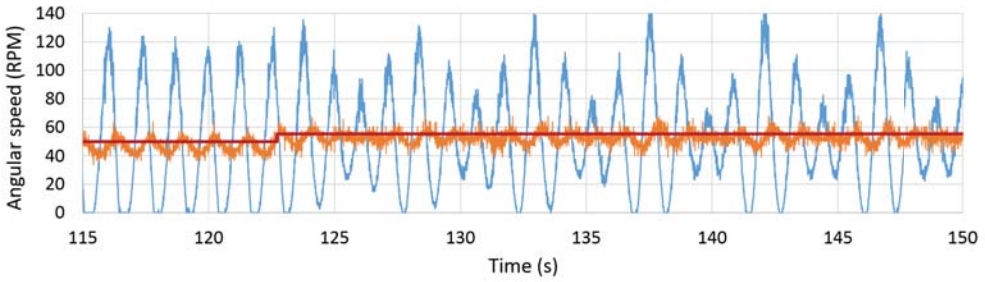

Figure 4.36: Influence of top drive speed on stick-slip from 115s to 150s

From 140s to 170s (fig. 4.37) one can see that the increase on the top drive speed from 55 RPM to 60 RPM eliminates the stick phase of the movement. Despite the presence of a severe torsional vibration on the system, the speed of J_1 does not becomes zero.

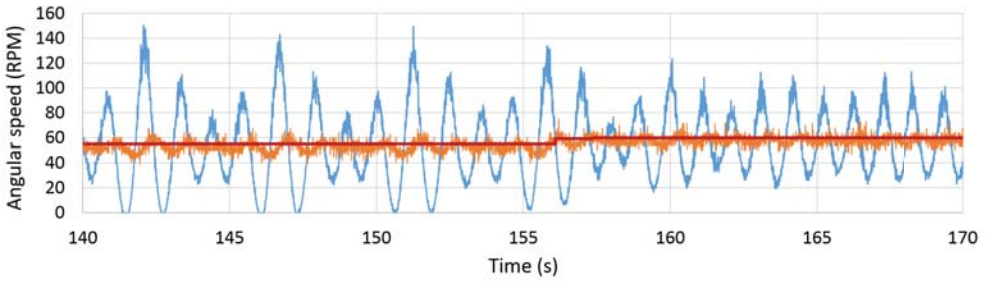

Figure 4.37: Influence of top drive speed on stick-slip from 140s to 170s

From the above figures one can see that the stick slip in the experimental setup is highly dependent of the angular velocity of the top drive. This behavior comes from the imperfections and misalignments of the setup and indicate that more complex friction laws should be considered for future works.